Advanced constitutive models in sheet metal forming

Proceedings
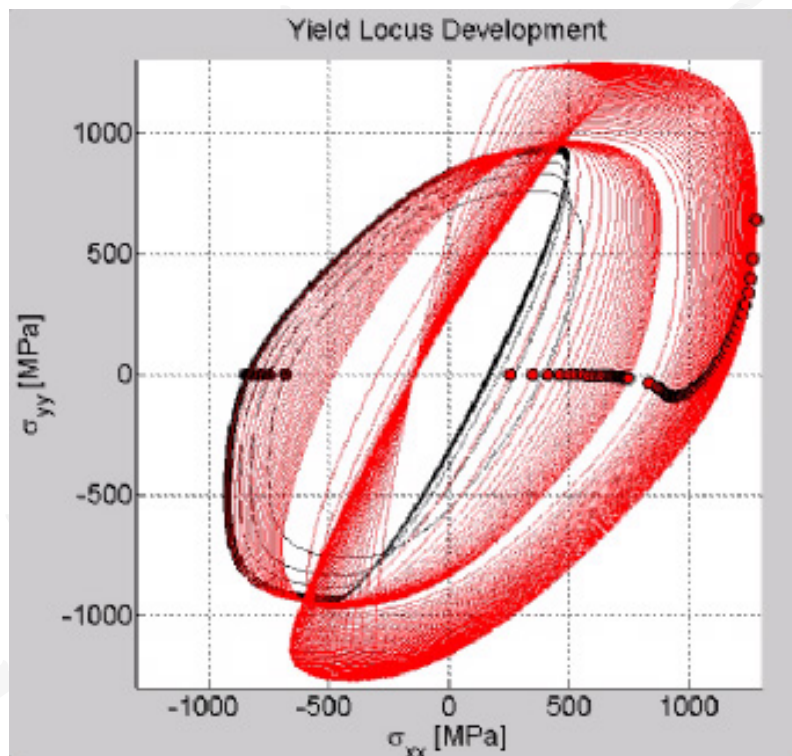
June 29 & 30, 2015
Zurich, Switzerland

Institut für Virtuelle Produktion
Institute of Virtual Manufacturing

ETH zürich

swddrg
Swiss Group of IDDRG

TUM
Technische Universität München

UNIVERSITY OF TWENTE.

Imprint

Institut für Virtuelle Produktion
Institute of Virtual Manufacturing

DIFFERENTIAL HARDENING IN IF STEEL
EXPERIMENTAL RESULTS AND A CRYSTAL PLASTICITY BASED MODEL

Hans Mulder[1,2], Philip Eyckens[3], Ton van den Boogaard[2*]

[1]Tata Steel, Research & Development, PO Box 10000,
1970 CA IJmuiden, The Netherlands
[2]University of Twente, Nonlinear Solid Mechanics, PO Box 217,
7500 AE Enschede, The Netherlands
[3]KU Leuven, Department of Materials Engineering, Kasteelpark Arenberg 44 - box 2450,
3001 Heverlee, Belgium

ABSTRACT: Work hardening in metals is commonly described by isotropic hardening, especially for monotonically increasing proportional loading. The relation between different stress states in this case is determined by equivalent stress and strain definitions, based on equal plastic dissipation. However, experiments for IF steel under uniaxial and equibiaxial conditions show that this is not an accurate description.

In this work, the determination of the equibiaxial stress–strain relation with 3 different tests will be elaborated: a stack compression test, a cruciform tensile test and a bulge test. A consistent shape of the hardening curve is obtained which deviates from that of a uniaxial tensile test.

Several physical explanations based on crystal plasticity are considered, including texture evolution, strain inhomogeneity and glide system hardening models. Texture evolution changes the shape of the yield surface and hence causes differential hardening, however, the observed differences at low strains cannot be explained by texture evolution. Accounting for the strain heterogeneity in the polycrystal, with equilibrium of forces over grain boundaries, improves the prediction of differential hardening considerably, even with a simplified interaction model (Alamel) and simple hardening laws for the glide systems. The presentation is based on a recently published paper by the authors [1].

KEYWORDS: Anisotropic hardening, Yield condition, Crystal plasticity

1   INTRODUCTION

Differential hardening is defined after Hill and Hutchinson [2] as the phenomenon that the stress-strain behaviour of a metal in case of proportional, monotonic loading conditions cannot be described by a single hardening curve based on the dissipated plastic work, but rather depends on the loading condition. The cause for this behaviour is commonly accepted to be texture development and non-isotropic hardening is thus expected to occur at relatively high deformations.

Mulder and Vegter [3] recently observed that the hardening behaviour of steel in the first few percent of deformation is highly non-isotropic. An observation that is generally found by the authors for all steel grades and which appears to be more apparent for strongly textured materials, e.g. like the IF steel grade in Fig. 1.

The first part of the presented work demonstrates the accuracy of the equibiaxial hardening curve.

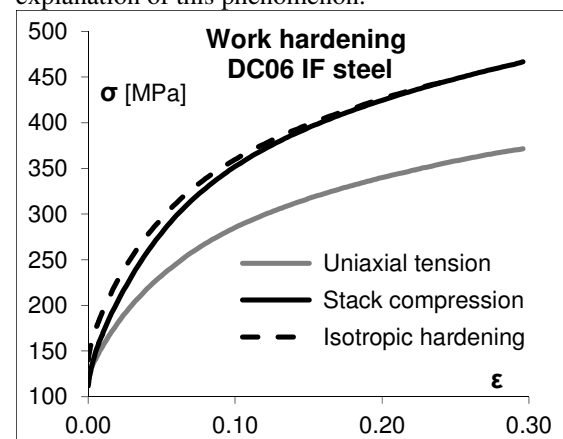The second part works towards a metallurgical explanation of this phenomenon.

Fig. 1   *Differential hardening at the onset of deformation for an IF steel grade*

The dotted line in Fig. 1 shows the equibiaxial hardening curve when isotropic hardening is assumed and the stress ratio (σ/σ_{un} at equal levels of

plastic work) is established towards the end of uniform strain in the tensile test.

2 EQUIBIAXIAL TENSION TESTS

Looking at Fig. 1 the first question is how accurate the equibiaxial hardening curve is established, especially at the low strain range. Three methods have been used to establish the flow curve under equibiaxial stress conditions:

1. The Biaxial Tensile Test (BTT). This test is performed at the Materials Mechanics Laboratory of POSTECH on a Kokusai KBAT-100 in-plane biaxial tensile testing machine. The design of the machine as well as the cruciform specimen are documented in a paper by Kuwabara et al. [4].

2. The Stack Compression Test (SCT). This test uses cubic specimens made from laminated sheet samples that are compressed in the through-thickness direction. The equipment and the sample are documented in An and Vegter [5].

3. The Hydraulic Bulge Test (HBT). This test is performed at Tata Steel using a die diameter of 200 mm and an optical measuring system. The test setup is described in the draft standard ISO16808. Data processing is documented in Mulder et al. [6].

2.1 FLOW STRESS RESULTS

The flow stresses for the three tests are shown in Fig. 2. Presented curves are the averages of 2 or 3 samples.
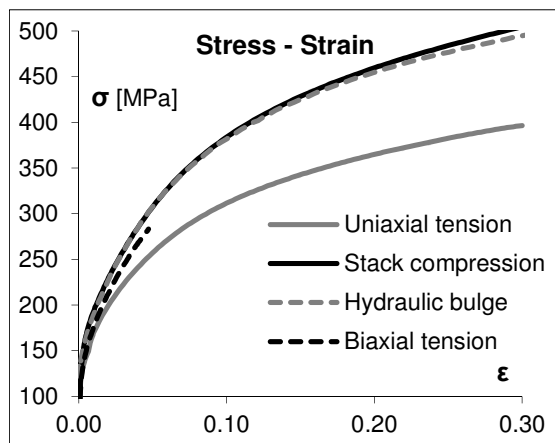

Fig. 2 *Flow stresses for equibiaxial tests*

The influence of friction on the SCT is reduced by using oiled teflon film between cube and tools. The barrel shape is negligible up to strains of 0.5. The accuracy of this test is further enhanced by using extensometers to measure the strains in rolling direction (RD) and tangential direction (TD) on the symmetry plane of the cube. The pressure in the symmetry plane may not be fully uniform in case of barreling, but there are no shear stresses.

2.2 WORK HARDENING

The results for the flow stress are established at different process conditions, in particular at different strain rates and temperature. A model is needed to compensate for these dynamic effects and compare the results at comparative conditions.

Mecking and Kocks [7] have shown that contributions to the flow stress of metallic materials are in general additive.

$$\sigma_f = \sigma_w(\varepsilon) + \sigma_d(\dot{\varepsilon}, T) \qquad (1)$$

In this classical abstraction the plastic behaviour is divided into two mechanistic steps. The flow stress depends on the current structure. The current dislocation structure is assumed to be represented by a single parameter, the dislocation density (ρ), and this structure develops with strain. The threshold level at which dislocation multiplication (i.e. plastic deformation) starts, depends on strain rate and temperature.

The structure development will also be rate dependent but for the common temperature range of cold forming that can be neglected.

The dynamic stress component can be derived from the concept of thermally activated dislocation glide:

$$\sigma_d(\dot{\varepsilon}, T) = \sigma_0^* \left(1 + \frac{k_B T}{\Delta G_0} ln \frac{\dot{\varepsilon}}{\dot{\varepsilon}_m}\right)^m \qquad (2)$$

In this equation σ_0^* is the maximum dynamic stress, usually in the order of 600 MPa, k_B is Boltzmann's constant ($8.617.10^{-5}$ eV/K), ΔG_0 is the maximum Gibbs free energy (0.8 eV) and $\dot{\varepsilon}_m$ is the maximum strain rate (1.10^8 /s).

The temperature in a test can either be measured independently or be established from a calibrated model, e.g. as in [8] for the bulge test. Using the temperature and strain rate data for the individual tests the following comparative data is obtained.
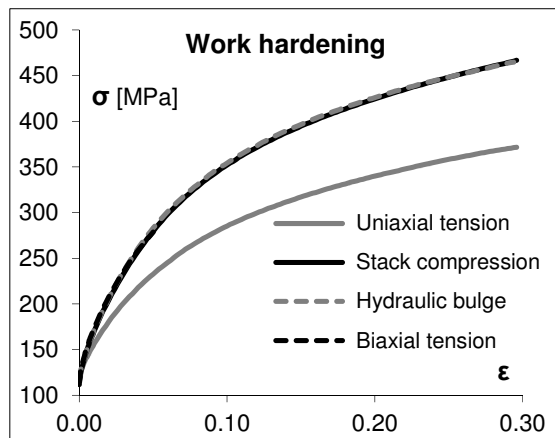

Fig. 3 *Work hardening for equibiaxial tests*

The curves for all three tests are indicating the same work hardening behaviour. The equibiaxial hardening curve in Fig. 1 is indeed accurate.

2.3 YIELD POINT

The major contribution in the transformation from Fig. 2 (flow stress) to Fig. 3 (work hardening) is due to the compensation of the stress for strain rate and temperature. A minor contribution is due to the change from total strain to plastic strain.

Van Liempt and Sietsma [9] subdivide the pre-yield strain in a linear elastic strain and a non-linear anelastic strain. The anelastic behaviour is largely due to orientation differences between neighbouring grains. Dislocation multiplication marks the start of plastic deformation. This start of plasticity can be recognized using a Kocks-Mecking analysis of the test results.
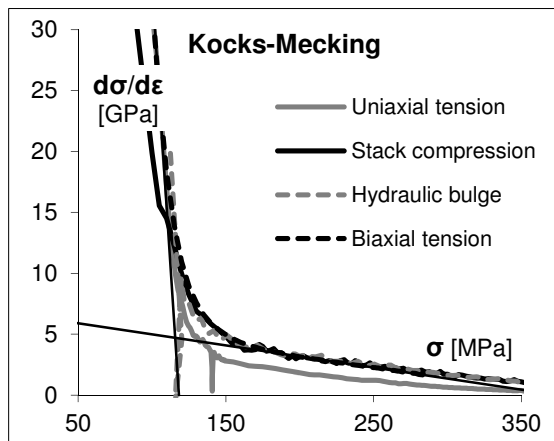

Fig. 4 *Yield point from Kocks-Mecking analysis*

The point where the two tangent lines cross indicates the yield strength.

Due to the nature of the tests the analysis results for the stack compression test and the hydraulic bulge test are debatable. It is remarkable that they nevertheless coincide quite well with the biaxial tensile test.

The plastic strain is obtained by subtracting both the elastic strain and the non-linear anelastic strain that is found for the yield stress.

3 DIFFERENTIAL HARDENING

In the isotropic hardening assumption there is one curve that describes the hardening behaviour for a reference stress state, usually uniaxial tension. The yield locus describes the stress ratio at which plastic deformation starts for arbitrary loading conditions relative to a reference condition, the equivalent stress. Hardening for stress states other than the reference is established based on the amount of plastic work. A dislocation structure with a certain dislocation density will have taken a fixed amount of energy, irrespective of the stress state for the deformation.

For proportional, monotonic loading conditions (like the uniaxial and equibiaxial tests) the stress ratio, and thus the shape of the yield locus, are assumed to be constant. The hardening curve that would appear for an equibiaxial test in this assumption is shown in Fig. 1 as a dotted line. The actual stress ratio derived from the work hardening curves in Fig. 3 are shown in Fig. 5.
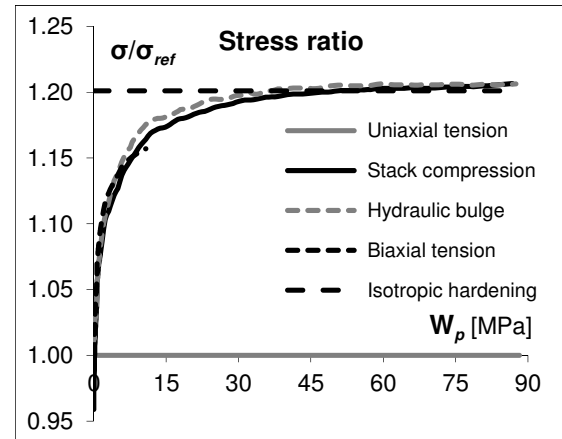

Fig. 5 *Stress ratio for equibiaxial tests*

Fig. 5 shows much clearer than Fig. 1 how the material behaviour deviates from isotropic hardening. The stress ratio for the uniaxial test is 1.0 as this is also the reference. An isotropic hardening material would have a constant stress ratio for the equibiaxial stress state, as shown by the straight dotted line. The strong development of the actual stress ratio at the start of deformation is remarkable because the commonly referenced cause for differential hardening is texture development. It is therefore expected to be fairly constant at the start of deformation with a gradual deviation towards higher deformation levels.

Possible causes (explanations) for this differential hardening behaviour at the start of deformation are:

1. A strain path change. Sheet metals have typically passed a temper mill and a stretcher-leveller as last deformation steps in manufacturing. Both are (small) plane strain deformations and uniaxial tension deviates from that in the opposite direction as equibiaxial tension. This hypothesis is easily disproven by a simple test: sheet metal before temper rolling and stretcher-levelling shows exactly the same behaviour.

2. The previously mentioned anelastic pre-yield behaviour [9] considers the presence of stress gradients near grain boundaries due to anisotropic elasticity. It is yet unclear to what extent these stress gradients will continue to influence material behaviour after dislocation multiplication (yielding).

3. Texture development and slip partitioning. As stated before it is generally accepted that texture development is the root cause for differential hardening when gradual changes at high deformation

are observed. It is unlikely that texture development is the only explanation for the observed behaviour. Being dependent on the orientation, the partitioning of the local strain via slip over the different slip systems will generally evolve as a consequence of texture evolution. This may have more impact at the start of deformation than expected.

4. Development of strain heterogeneity. Individual grains will have a strain dependence on texture, microstructure and load case, which need not be identical to the macro strain. It is also known that intra-granular strain heterogeneities exist. These strain heterogeneities contribute to the anisotropic behaviour. If the strain heterogeneity changes with deformation it may contribute to differential hardening.

5. Development of the critical resolved shear stress. Hardening is known to depend on the number of dislocations. The number of dislocations is driven by micro strain and available slip systems, in other words grain (orientation) dependent. The critical resolved shear stress may therefore develop differently for each grain and contribute to developments in strain heterogeneity.

The first possible explanation is disproven by a straightforward test. The second possible explanation requires the addition of anisotropic elasticity to a crystal plasticity framework. The last three explanations have been modelled in a statistical crystal plasticity model. Simulations will give an indication of their individual contribution to the observed phenomenon.

4 CRYSTAL PLASTICITY

Crystal plasticity models can be classified in *full-field* and *statistical* models.

Full-field crystal plasticity models make use of a Representative Volume Element (RVE) of the microstructure, which is sufficiently large so that the average response of the RVE to a particular loading would correspond to that of the material at the macroscopic level. Different numerical methods have been used to solve the non-linear plasticity problem of the RVE. The most common is the Finite Element Method (CP-FEM). More recently the Fast Fourier Transform method (CP-FFT) is gaining in popularity because the calculation time is generally much shorter.

Statistical crystal plasticity models build upon the knowledge of the statistical distribution of crystallographic orientations of the material. A representative set of crystals is typically derived from the Orientation Distribution Function (ODF). Compared to full-field models, statistical crystal plasticity models make further abstraction of the microstructure while attempting to capture the most significant effects of microstructure on the macroscopic behaviour. This allows them to be considerably faster than full-field methods.

The classical statistical method is the one of Taylor-Bishop-Hill (TBH, also called the Taylor model). The basic *Taylor* model assumes a homogeneous deformation of all crystals. In other words the micro strain for individual crystals is equal to the macro strain. As a consequence the stress equilibrium along the boundaries of neighbouring grains is generally not satisfied. This limitation is the main reason why deformation textures predicted by the TBH theory only qualitatively agree with experimental deformation textures. Grain interaction models formulate certain relaxations on the strict Taylor assumption, thereby improving the stress equilibrium condition along grain boundaries. The *Alamel* model, Van Houtte et al. [10], considers a bicrystal, i.e. a grain boundary and two crystals at either side. This model is extensively validated by deformation texture predictions for steel. The Alamel model is also known to predict a more realistic initial yield locus compared to the Taylor model. The hardening and stress ratio predictions in this paper compare both the Taylor and the Alamel model with the experimental results as shown in Figs. 3 and 5.

4.1 CRITICAL RESOLVED SHEAR STRESS

Any non-zero local plastic strain rate needs to be realized through plastic deformation, which is carried by dislocation slip on a number of slip systems. Dislocation slip on a slip system (s) is described by simple shear on the slip plane. The amount of slip per unit time is given by the shear rate $\dot{\gamma}^{(s)}$. The simultaneous slipping of a number of slip systems realizes the plastic strain rate inside a grain.

For ferritic (BCC) steels 24 slip systems are assumed to be potentially active: 12 {110}<111> and 12 {112}<111> slip systems. The imposed strain rate tensor has however only 5 independent components, considering it is symmetric and traceless due to plastic incompressibility. Thus an infinite number of solutions exist. Taylor proposed to retain the solutions with minimal dissipation of plastic work. The plastic work in the crystal per unit volume is given by

$$p = \sum_{(s)} \tau_c^{(s)} \left| \dot{\gamma}^{(s)} \right| \tag{3}$$

Here the critical resolved shear stress (CRSS) of a slip system, $\tau_c^{(s)}$, is the scalar measure of stress that is work-conjugate to the respective slip rate $\dot{\gamma}^{(s)}$. In principle the CRSS may be different for the two considered slip system families due to the different atomic configuration in {110} and {112} planes. It may also be different between forward and reverse slip on {112} slip planes (stress differential effect). Moreover the development of an anisotropic cell

substructure with ongoing plastic deformation will generally lead to different values of CRSS between the individual slip systems and also between the two slip directions for a particular slip system (development of back stress). In this paper however all these differences are neglected and it is assumed that inside each grain the CRSS is the same for all slip systems. Hence Eqn. 3 reduces to

$$p = \tau_c \sum_{(s)} |\dot{\gamma}^{(s)}| = \tau_c \dot{\Gamma} \tag{4}$$

in which $\dot{\Gamma}$ is the total slip rate inside the grain. The accumulated slip within a grain is obtained through time integration of the grain slip rate:

$$\Gamma = \int \dot{\Gamma} dt \tag{5}$$

A *microscopic* strain hardening relation postulates the evolution of the CRSS inside a grain as a Swift-type hardening function of the accumulated slip of that grain.

$$\tau_c(\Gamma) = \tau_0(\Gamma + \Gamma_0)^n \tag{6}$$

Macroscopic strain hardening assumes that the CRSS is identical for each constituting grain at any given time. An obvious choice for the strain parameter in the hardening equation is the volume-average accumulated slip $\bar{\Gamma}$:

$$\tau_c(\bar{\Gamma}) = \tau_0(\bar{\Gamma} + \Gamma_0)^n \tag{7}$$

We have defined 4 variants for the statistical crystal plasticity model: (Taylor, micro), (Taylor, macro), (Alamel, micro) and (Alamel, macro), with which we investigate the possible causes for differential hardening as mentioned in chapter 3.
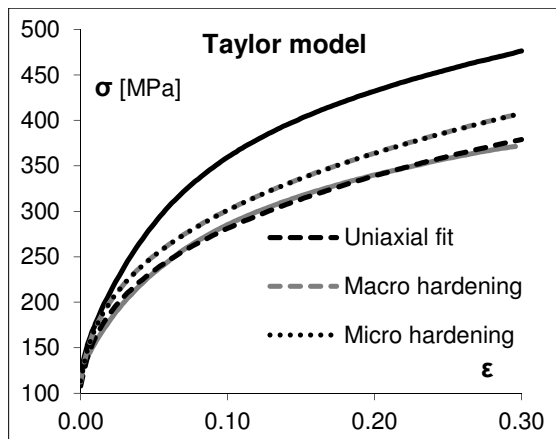
4.2 SIMULATION RESULTS

Fig. 6   *Taylor model simulation results*

The hardening parameters τ_0, Γ_0 and n are tuned separately for each of the 4 model variants to fit the uniaxial tension hardening curve in Fig. 3. The simulation of equibiaxial tension is performed with the fitted hardening parameters. The experimental stack compression results are included in Figs. 6 and 7 for reference as a continuous black line.
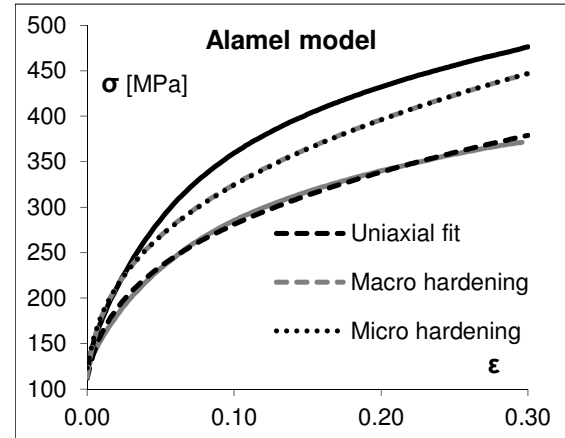
Fig. 7   *Alamel model simulation tests*

The stress ratio that result from the simulations are shown in the following figure.
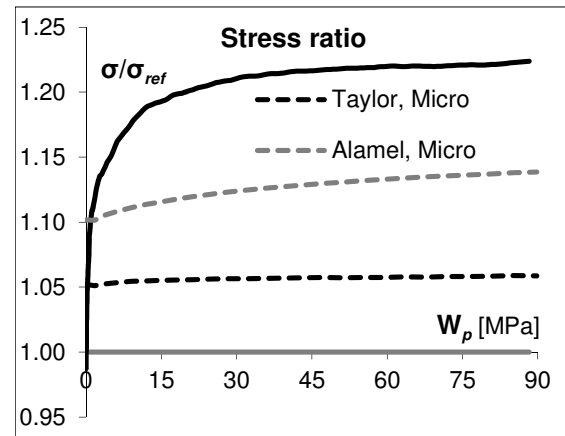
Fig. 8   *Stress ratio from simulation tests*

4.3 DISCUSSION

On first observation the Alamel model is much better at predicting equibiaxial hardening than the Taylor model, but there is still a significant difference with experimental results. And despite the fact that microscopic hardening reflects the physical process of strain hardening through dislocation multiplication much better, there is hardly a difference with macroscopic strain hardening simulations. Possible explanation 5 in chapter 3 is therefore unlikely.

In a recently published paper by the authors [1] two other steel grades were included in the research. The Alamel model was much more accurate in predicting equibiaxial hardening and the corre-

sponding stress ratio for these steel grades. The stress equilibrium condition at grain boundaries is apparently very important for hardening predictions in different load cases. The deformation relaxation of the Alamel model (compared to the Taylor model) is probably a good average approximation, however it might be insufficient for strongly textured grades. Full-field crystal plasticity models have an inherent advantage in this respect. Comparing the Taylor simulation results with the Alamel results it is likely that a better simulation of the strain heterogeneity, considering the stress equilibrium condition at grain boundaries, will improve the average level of the stress ratio (Fig. 8) but it will not explain the steep inclination of the stress ratio between 0 and 30 MPa plastic work.

The Alamel model is good at predicting deformation textures. The gradual increase of the stress ratio between 30 and 90 MPa in Fig. 8 is predicted by the Alamel model whereas the Taylor model shows a flat line. Texture development is confirmed as a root cause for differential hardening when a gradual change at higher deformations is considered. Possible explanation 2 remains as the most likely cause for the steep change in stress ratio at the start of deformation.

5 CONCLUSIONS

1. The stress equilibrium condition at grain boundaries and the corresponding impact on strain heterogeneity at the grain size level plays a key role in the accurate prediction of hardening for textured single phase steels. The Alamel model doesn't capture this phenomenon in full for the steel grade in this paper, but it did for two other grades in [1].

2. Texture development plays an important role in the prediction of differential hardening. Texture evolution changes the shape of the yield locus. The Alamel model has been developed and is validated for the prediction of deformation texture.

3. Prescribing the evolution of the CRSS at the individual grain level (microscopic hardening) leads to very similar results as prescribing one CRSS for the polycrystal (macroscopic hardening).

4. The remarkable steep increase of the stress ratio at the start of deformation is not explained by the current simulations. Possible explanations that remain are loading dependent dislocation substructures and the local stresses near grain boundaries as a result of anisotropic elasticity.

6 ACKNOWLEDGEMENT

REFERENCES

[1] Eyckens P., Mulder H., Gawad J., Vegter H., Roose D., Van den Boogaard T., Van Bael A., Van Houtte P.: *The prediction of differential hardening behaviour of steels by multi-scale crystal plasticity modelling*. International Journal of Plasticity, in press, http://dx.doi.org/10.1016/j.ijplas.2014.12.004.

[2] Hill R., Hutchinson J.W.: *Differential hardening in sheet metal under biaxial loading: a theoretical framework*. Journal of Applied Mechanics 59, S1-S9, 1992.

[3] Mulder J., Vegter H.: *Evolving anisotropic yield loci based on multiple hardening curves*. In: 13th ESAFORM Conference on Material Forming, 2010.

[4] Kuwabara T., Ikeda S., Kuroda K.: *Measurement and analysis of differential work hardening in cold-rolled steel sheet under biaxial tension*. Journal of Materials Processing Technology 80-81, 517-523, 1998.

[5] An Y.G., Vegter H.: *Analytical and experimental study of frictional behavior in through-thickness compression test*. Journal of Materials Processing Technology 160, 148-155, 2005.

[6] Mulder J., Vegter H., Aretz H., Keller S., Van den Boogaard A.H.: *Accurate determination of flow curves using the bulge test with optical measuring systems*. Submitted, 2015.

[7] Mecking H., Kocks U.F.: *Kinetics of flow and strain hardening*. Acta Metallurgica 29, 1865-1875, 1981.

[8] Mulder J., Vegter H., Van den Boogaard A.H.: *An engineering approach to strain rate and temperature compensation of the flow stress established by the hydraulic bulge test*. In: 18th ESAFORM Conference on Material Forming, 2015.

[9] Van Liempt P., Sietsma J.: *A physically based yield criterion for plastic deformation in metals*. Submitted, 2015.

[10] Van Houtte P., Li S., Seefeldt M., Delanney L.: *Deformation texture prediction: from the Taylor model to the advanced Lamel model*. International Journal of Plasticity 21, 589-624, 2005.